VOLUME 123, NUMBER 51
DECEMBER 26, 2001

JOURNAL OF THE AMERICAN CHEMICAL SOCIETY

Toward the de Novo Design of a Catalytically Active Helix Bundle: A Substrate-Accessible Carboxylate-Bridged Dinuclear Metal Center

Luigi Di Costanzo,[†] Herschel Wade,[‡] Silvano Geremia,*[,†] Lucio Randaccio,[†] Vincenzo Pavone,[§] William F. DeGrado,*[,‡] and Angela Lombardi*[,§]

Contribution from the Biocrystallography Centre of Excellence, Department of Chemical Science, University of Trieste, Via L. Giorgieri 1, I-34127 Trieste, Italy, Department of Biochemistry and Biophysics, University of Pennsylvania School of Medicine, Philadelphia, Pennsylvania 19104-6059A, and Department of Chemistry, University of Napoli ''Federico II'', Complesso Universitario Monte S. Angelo, Via Cynthia 45, I-80126 Napoli, Italy

Received February 26, 2001

Abstract: De novo design of proteins provides an attractive approach to uncover the essential features required for their functions. Previously, we described the design and crystal structure determination of a di-Zn(II) complex of "due-ferri-1" (DF1), a protein patterned after the diiron−dimanganese class of redox-active proteins [Lombardi, A.; Summa, C.; Geremia, S.; Randaccio, L.; Pavone, V.; DeGrado, W. F. *Proc. Natl. Acad. Sci. U.S.A.* **2000**, *97*, 6298−6305]. The overall structure of DF1, which contains a carboxylate-bridged dinuclear metal site, agrees well with the intended design. However, access to this dimetal site is blocked by a pair of hydrophobic leucine residues (L13 and L13′), which prevent facile entry of metal ions and small molecules. We have now taken the next step in the eventual construction of a catalytically active metalloenzyme by engineering an active site cavity into DF1 through the replacement of these two leucine residues with smaller residues. The crystal structure of the dimanganous form of L13A-DF1 indeed shows a substrate access channel to the dimetal center. In the crystal structure, water molecules and a ligating dimethyl sulfoxide molecule, which forms a monatomic bridge between the metal ions, occupy the cavity. Furthermore, the diferric form of a derivative of L13A-DF1, DF2, is shown to bind azide, acetate, and small aromatic molecules.

Introduction

The design of metalloproteins provides an attractive approach to test the essential features required for folding, electron transfer, and catalysis.[1,2] This problem has been approached through the introduction of novel metal binding sites into naturally occurring proteins[3] as well as through de novo protein design.[4,5]

We have divided the problem of designing catalytic metalloproteins into several parts: the first involves the design of stable, uniquely folded proteins that contain metal binding sites. This is followed by the engineering of a substrate recognition

* To whom correspondence should be addressed. E-mail: lombardi@chemistry.unina.it; wdegrado@mail.med.upenn.edu; geremia@univ.trieste.it.
† University of Trieste.
‡ University of Pennsylvania.
§ University of Napoli.

(1) Anderson, K. K.; Elgren, T. E.; Que, L., Jr.; Lipsomb, J. D. *J. Am. Chem. Soc.* **1992**, *114*, 8711−8712.
(2) Que, L. *Coord. Chem. Rev.* **1983**, *50*, 73−108.
(3) Hellinga, H. W. *Folding Des.* **1998**, *3*, R1−R8.
(4) Lombardi, A.; Summa, C.; Geremia, S.; Randaccio, L.; Pavone, V.; DeGrado, W. F. *Proc. Natl. Acad. Sci. U.S.A.* **2000**, *97*, 6298−6305.
(5) DeGrado, W. F.; Summa, C. M.; Pavone, V.; Nastri, F.; Lombardi, A. *Annu. Rev. Biochem.* **1999**, *68*, 779−819.

10.1021/ja010506x CCC: $20.00
Published on Web 12/19/2001

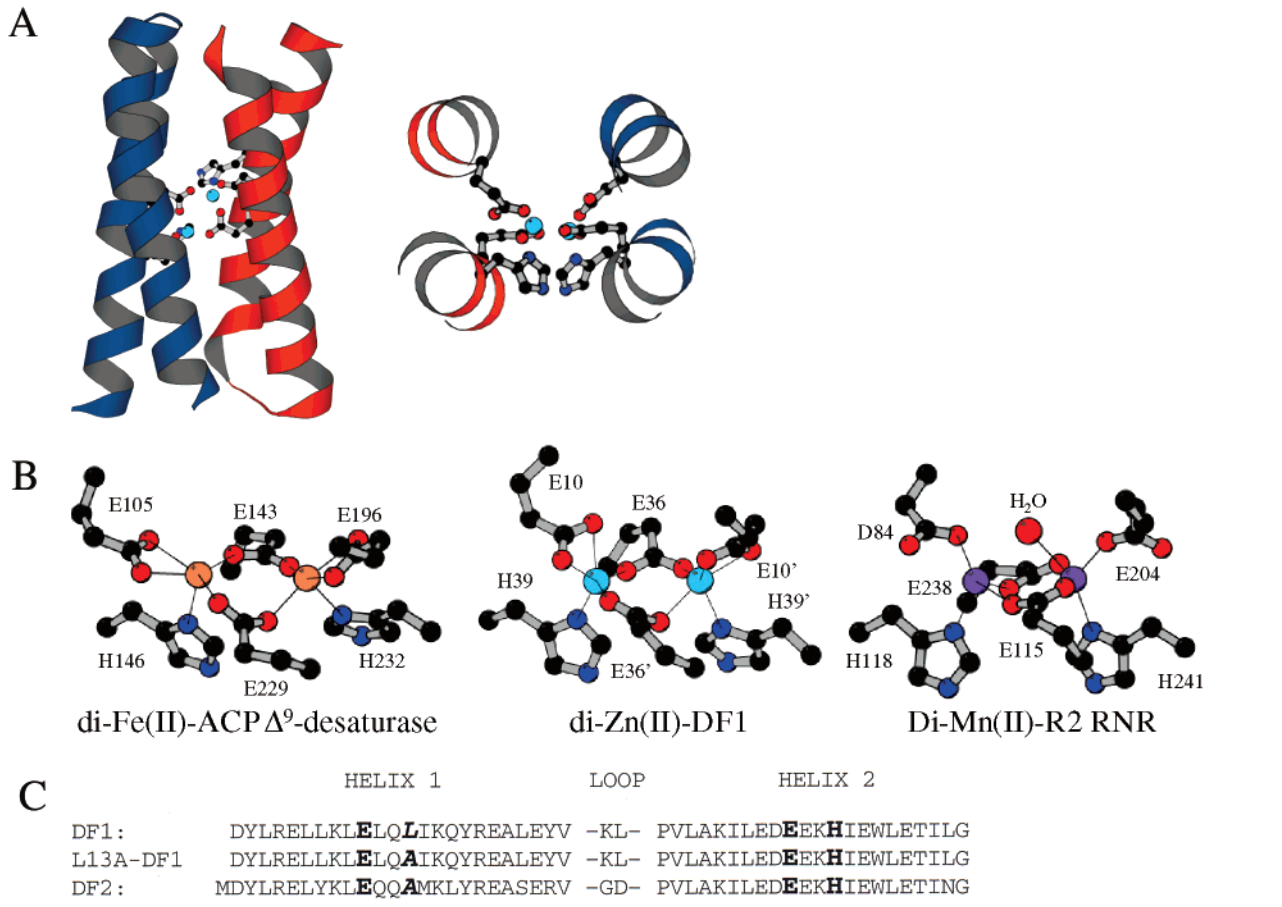

Figure 1. Crystal structure of di-Zn(II)-DF1. (A) Side view and top view of the helix−turn−helix homodimer (monomers are colored orange and blue) shown with the liganding residues and the active site Zn^{2+} metal ions (light blue). (B) Dinuclear metal centers of two natural proteins, ACP Δ^9-desaturase (left) and the manganese-substituted R2 subunit of the *E. coli* ribonucleotide reductase (right), along with the di-Zn(II)-DF1 (middle). (C) Amino acid sequences of due-ferri-1 DF1, DF2, and L13A-DF1. The active site ligands are highlighted in bold, and the Leu to Ala change is shown in italics. Part A and the active site structures were generated with Molscript.[69]

site that is capable of binding small molecules proximal to the metal center. The geometry, chemical reactivity, and electronic properties of the metal center can then be finely tuned to provide a desired catalytic function. The first objective has been established through the design of due-ferri-1 (DF1),[4,6] a protein-based, minimal model for diiron and dimanganese proteins.[7−10] Originally, the core of DF1 was filled with hydrophobic residues which efficiently pack in a geometrically complementary manner to provide thermodynamic stability and conformational uniqueness.[4] Although this strategy was successful in producing a stable, nativelike protein, the design of DF1 had several shortcomings. To constitute the metallo active site, DF1 must be denatured and refolded in the presence of metal ions, indicating that the folded form of the protein does not provide access to its active site. In addition, computer modeling indicated that DF1 lacks a cavity to bind small molecule substrates proximal to the metal binding site. Here, we describe the successful introduction of an active site cavity into the structure of DF1.

DF1 (Figure 1A) is a noncovalently associated homodimer of two helix−loop−helix hairpin motifs, which idealizes the pseudo-2-fold symmetry observed in natural diiron and dimanganese proteins.[11] The two metal ions are bound near the center of the four-helical bundle and are bound with ligation geometries very similar to those found for the metal ions in the reduced forms of natural diiron and dimanganese proteins.[12−15] Each individual Zn^{2+} ion has three glutamate ligands and one histidine ligand (Figure 1B). Two of the glutamate carboxylates (E36 and E36′) form μ-1,3 syn-syn bridging interactions with the metal ions while the other two (E10 and E10′) interact with individual ions in a bidentate chelating manner. Two histidine residues (H39 and H39′) complete the primary coordination sphere to the Zn^{2+} ions via their Nδ atoms. This pentacoordinate ligand arrangement is nearly identical to that observed in the crystal structure of the dinuclear metal sites of di-Fe(II) ACP Δ^9-desaturase[13] and di-Mn(II) bacterioferritin[16] and is similar to the center in the di-Mn(II)-substituted R2 subunit of ribo-

(6) Hill, R. B.; Raleigh, D. P.; Lombardi, A.; DeGrado, W. F. *Acc. Chem. Res.* **2000**, *33*, 745−754.
(7) Nordlund, P.; Eklund, H. *Curr. Opin. Struct. Biol.* **1995**, *5*, 758−766.
(8) Lange, S. J.; Que, L., Jr. *Curr. Opin. Chem. Biol.* **1998**, *2*, 159−172.
(9) Feig, A. L.; Lippard, S. J. *Chem. Rev.* **1994**, *94*, 759−805.
(10) Kurtz, D. *J. Biol. Inorg. Chem.* **1997**, *2*, 159−167.
(11) Summa, C. M.; Lombardi, A.; Lewis, M.; DeGrado, W. F. *Curr. Opin. Struct. Biol.* **1999**, *9*, 500−508.
(12) Logan, D. T.; Su, X.-D.; Aberg, A.; Regnstrom, K.; Hajdu, J.; Eklunnd, H.; Norland, P. *Structure* **1996**, *4*, 1053−1062.
(13) Lindqvist, Y.; Huang, W.; Schneider, G.; Shanklin, J. *EMBO J.* **1996**, *15*, 4081−4092.
(14) Atta, M.; Nordlund, P.; Aberg, A.; Eklund, H.; Fontecave, M. *J. Biol. Chem.* **1992**, *267*, 20682−20688.
(15) Rosenzweig, A. C.; Nordlund, P.; Takahara, P. M.; Frederick, C. A.; Lippard, S. J. *Chem. Biol.* **1995**, *2*, 409−418.
(16) Frolow, F.; Kalb (Gilboa), A. J.; Yariv, J. *Nat. Struct. Biol.* **1994**, *1*, 453−460.

nucleotide reductase[14] (Figure 1B). In DF1 and these natural proteins, two adjacent vacant coordination sites, both trans to the liganding histidine residues, are well positioned to interact with substrates such as O_2 and H_2O_2. Closer examination of the DF1 crystal structure indicated that the side chains of L13 and L13′ block access to these vacant coordination sites. Moreover, computer modeling suggested that the substitution of two leucine residues (L13 and L13′) with alanine or glycine residues would lead to the formation of a cavity large enough to allow small molecules access to the metal center. Indeed, the natural diiron and dimanganese proteins tend to have small side chains at these positions. We therefore synthesized L13A-DF1 and undertook its structural characterization.

To extend these crystallographic studies, we have also examined the ligand binding and spectroscopic properties of DF2, a closely related derivative of L13A-DF1. Although L13A-DF1's limited solubility in aqueous solution has facilitated the formation of diffraction-quality crystals, it has impeded further solution characterization in the absence of organic solvents. We have therefore designed a more water-soluble version of L13A-DF1 and have expressed it in *Escherichia coli*. This protein, DF2 (see Figure 1C for the DF1, L13A-DF1, and DF2 sequences), also has an alanine side chain at an analogous position to residue 13 of L13A-DF1, and its metal ion binding properties have been extensively studied.[17] In contrast to DF1, DF2 can be reconstituted with metal ions without unfolding the apoprotein, suggesting that the metal binding site is readily accessible to small molecules. DF2 also shows modest ferroxidase activity,[17] and preliminary data indicate that it forms an oxo-bridged diferric center, similar to those observed in the R2 subunit of ribonucleotide reductase,[18,19] methemerythrin,[20,21] ACP Δ^9-desaturase,[13] ferritin,[22,23] rubrerythrin,[24] and small molecule models for diiron proteins.[9,25]

Experimental Section

Methods and Material. L13A-DF1 was chemically synthesized by using standard Fmoc protocols and purified to homogeneity by RP-HPLC;[26] MALDI-TOF mass spectrometry gave the expected molecular weight (L13A-DF1: 5837 amu). DF2 was expressed and purified as described previously.[17]

Solution Studies. The di-Fe(III)-DF2 complex was prepared by first dissolving lyophilized DF2 into 50 mM MES and 100 mM NaCl, pH 6.5 buffer, at a protein concentration of 50−100 μM. From a ferrous ammonium sulfate stock solution (13 mM in 0.1% H_2SO_4), small aliquots (0.5 μL) were added in the presence of air every 15 min, until the Fe/DF2 dimer ratio was 2.1−2.2. After the complex was incubated with ambient oxygen for 1 h, the sample was centrifuged and/or filtered to remove a small amount of precipitated protein and iron oxides. The resulting solution was used for the titrations with small ligands. The di-Fe(III)-DF2 solutions were used the same day that they were prepared. All ligand stocks were prepared in the 50 mM MES and 100 mM NaCl buffer. When needed, HCl or NaOH was added to adjust the buffer to a final pH of 6.5. The spectra were measured on a Hewlett-Packard diode array spectrophotometer.

Table 1. Crystallographic Data for Di-Mn(II)-L13A-DF1

	form **1**	form **2**
X-ray source	Elettra	Elettra
wavelength (Å)	1.200	1.200
temperature (K)	100	100
space group	$P2_12_12_1$	$C222_1$
cell dimensions (Å)		
a	37.38	37.12
b	80.12	112.45
c	99.93	79.88
V (Å^3)	299300	333400
resolution (Å)	20.1−1.7	21.2−2.2
highest resolution shell (Å)	1.80−1.70	2.32−2.20
total reflections	177455	18643
unique reflections	33538	7562
$I/\sigma(I)$[a]	14.0 (2.9)	7.5 (2.2)
completeness (%)		
all data	99.4	87.3
last shell (Å)	96.6	90.5
multiplicity	5.3	2.5
R_{merge}[a,b]	9.6 (40.9)	10.7 (32.9)

[a] Values in parentheses refer to the highest resolution shell. [b] $R_{merge} = \sum\sum I(h)j - \langle I(h)\rangle / \sum\sum I(h)j$ where $I(h)$ is the measured diffraction intensity and the sum includes all reflections.

Crystallization Studies. L13A-DF1 was crystallized using poly(ethylene glycol) as precipitant in the presence of a 20-fold excess of Mn(II) using the hanging drop method. The purified protein, not completely soluble in water, was dissolved in DMSO to obtain a solution of 100 mg/mL concentration. The solution was diluted 10-fold with water and centrifuged to remove particulate material. The drops were prepared by adding 2 μL of protein solution to 2 μL of reservoir solution containing PEG 400 (form **1**), $Mn(CH_3COO)_2$, 0.03 M, and Tris-HCl, 0.1 M, pH 7.5. Diamond-shaped crystals of di-Mn(II)-L13A-DF1 (0.25 × 0.19 × 0.12 mm^3) grew within 14 days at 277 K. Crystals of L13A-DF1 were also obtained using PEG 200 (form **2**), and in another experiment, both forms **1** and **2** were found in the same batch using only PEG 400. Crystallographic data for both forms **1** and **2** are reported in Table 1. The protein was also crystallized with a stoichiometric amount of $Mn(AcO)_2$. These smaller crystals diffract to lower resolution.

X-ray diffraction data were collected at the Elettra Synchrotron (Trieste, Italy). Data were collected using a monochromatic radiation with a wavelength of 1.200 Å and a MAR Research 345 mm imaging plate as detector. Crystals of both forms were harvested into mother liquor with a small loop of fine rayon fiber and flash-frozen in a stream of N_2 at 100 K. The determination of unit cell parameters, integration of reflection intensities, and data scaling were performed using MOSFLM and SCALA from the CCP4 program suite.[27] The form **1** crystals of di-Mn(II)-L13A-DF1 diffracted to 1.70 Å resolution. The structure was solved by molecular replacement[28,29] using the coordinates of di-Zn(II)-DF1 as the starting model and refined to the present *R* and R_{free} of 19.7% and 24.8%, respectively (Table 2). The form **2** crystals of di-Mn(II)-L13A-DF1 diffracted to 2.15 Å resolution; the structure was refined to the present *R* and R_{free} of 24.7% and 31.8%, respectively (Table 2).

Results and Discussion

Previously, the structure of DF1 was solved with two Zn(II) ions bound at the active site.[4] In the current work, the structure

(17) Pasternak, A.; Kaplan, J.; Lear, J.; DeGrado, W. F. *Protein Sci.* **2001**, *10*, 958−969.
(18) Sjorberg, B.-M.; Loehr, T. M.; Sanders-Loehr, J. *Biochemistry* **1982**, *21*, 96−102.
(19) Petersson, L.; Graslund, A.; Ehrenberg, A.; Sjoberg, B.-M.; Reichard, P. *J. Biol. Chem.* **1980**, *255*, 6706−6712.
(20) Garbett, K.; Darnall, D. W.; Klotz, I. M.; Williams, R. J. P. *Arch. Biochem. Biophys.* **1969**, *103*, 419−434.
(21) Reem, R. C.; McCormick, J. M.; Richardson, D. E.; Devlin, F. J.; Stephens, P. J.; Musselman, R. L.; Solomon, E. I. *J. Am. Chem. Soc.* **1989**, *111*, 4688−4704.
(22) Bauminger, E. R.; Harrison, P. M.; Novak, I.; Treffry, A. *Biochemistry* **1989**, *28*, 5486−5493.
(23) Bauminger, E. R.; Harrison, P. M.; Novak, I.; Treffry, A. *Biochim. Biophys. Acta* **1991**, *1118*, 48−58.
(24) deMare, F.; Kurtz, D. M., Jr.; Nordlund, P. *Nat. Struct. Biol.* **1996**, *3*, 539−546.
(25) Sanders-Loehr, J.; Wheeler, W. D.; Shiemke, A. K.; Averill, B. A.; Loehr, T. M. *J. Am. Chem. Soc.* **1989**, *111*, 8084−8093.
(26) Choma, C. T.; Lear, J. D.; Nelson, M. J.; Dutton, P. L.; Robertson, D. E.; DeGrado, W. F. *J. Am. Chem. Soc.* **1994**, *116*, 856−865.
(27) *Collaborative Computational Project 4*, Collaborative Computational Project 4, Ed.; 1994; Vol. D50, pp 760−763.
(28) Navaza, J.; Saludjian, P. In *AMoRe: An automated molecular replacement program package*; Navaza, J., Saludjian, P., Eds.; Academic Press: New York, 1997; Vol. 276, pp 581−594.
(29) Navaza, J. *Acta Cystallogr.* **1994**, *A50*, 157−163.

Table 2. Data Refinement Statistics for Di-Mn(II)-L13A-DF1

	form **1**	form **2**
final refinement parameters		
resolution range (Å)	19.8−1.7	20.0−2.2
no. of reflections used	31811	7186
R^a	0.197	0.247
$R_{free}{}^b$	0.248	0.318
no. of protein atoms	2478	1239
no. of internal Mn ions	6	3
no. of external Mn ions	5	
no. of DMSO atoms	12	6
no. of water molecules	247	32
mean *B* values (Å^2)		
protein atoms	24.8	41.8
internal Mn ions	14.6	27.1
external Mn ions	35.3	
DMSO atoms	22.6	32.8
water molecules	38.8	43.9
rms deviation from ideal geometry		
bond lengths (Å)	0.030	0.029
bond angles (deg)	2.2	4.3

[a] $R = \sum|F_o - F_c|/\sum F_o$, where F_o and F_c are the observed and calculated structure factor amplitudes, respectively. [b] R_{free} was calculated from a randomly chosen subset of 5.0% of the reflections.

of the DF1 variant L13A-DF1 reconstituted with Mn(II) ions has been solved in two different crystal forms (**1** and **2**). Having the structure of this DF1 variant with a redox-active and thus a more chemically relevant metal ion allows for useful comparisons with the structures of several natural di-Mn(II) enzymes, including arginase[30] and manganese catalase.[31,32] The comparisons can be extended further to diiron-oxo proteins, as the three-dimensional structures of di-Mn(II)-substituted forms of the R2 subunit of ribonucleotide reductase[14] and bacterioferritin[16] are known. Interestingly, manganese and iron metal ions often function similarly in structurally similar proteins (e.g., FeSOD versus MnSOD).[33]

The structures of crystal forms **1** and **2** of di-Mn(II)-L13A-DF1 were solved by molecular replacement using the coordinates of di-Zn(II)-DF1 as a starting model and refined using data that extended to 1.70 and 2.20 Å resolution, respectively. In this paper, the highest resolution structure (form **1**) will be discussed. The asymmetric unit contains three dimers as shown in Figure 2. The structures of the dimers are nearly identical to that of di-Zn(II)-DF1 (rmsd of about 0.7 Å for the backbone atoms), with the greatest differences being located at the helix termini and the loops. The electron density of the metal binding site and the surrounding site is well defined (Figure 3).

Although L13A-DF1 crystallizes from solutions containing stoichiometric concentrations of Mn(II), an excess of the cation was found to improve the diffraction of the crystals, suggesting that the excess ions might be involved in intersubunit contacts in the crystal lattice. Indeed, dimers of L13A-DF1 within a given unit cell are linked by five "external" crystallographically independent Mn(II) ions (Figure 2), one of which was found to be disordered over two sites, each with half-occupancy. Two others link pairs of dimers with similar coordination spheres including water molecules and amino acid side chains. Another Mn(II) ion binds to a glutamate and a glutamine residue of one

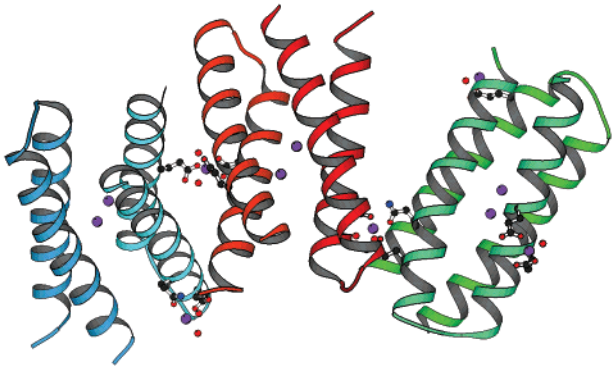

Figure 2. Three crystallographically independent dimers of the asymmetric unit. The amino acid residues and water molecules (red spheres) that coordinate nonactive site Mn(II) ions (violet spheres) are highlighted. The structure was generated with Molscript.[69]

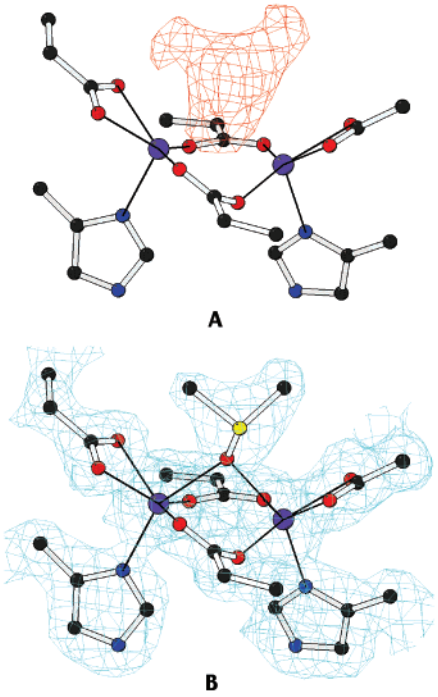

Figure 3. Electron density map of the dinuclear metal binding site of di-Mn-L13A-DF1. (A) $F_o - F_c$ omit map (contour levels are 3σ) depicting the density of the trilobate peak assigned to a DMSO ligand. (B) $2F_o - F_c$ map (contour levels are 1σ) for the liganding residues including the exogenous DMSO ligand.

monomer along with two water molecules, whereas the fifth binds to two glutamate residues of one monomer along with one water molecule. The external manganese ions affect the local conformation around the coordinated glutamates differently for each dimer but have minimal effect on the active site conformation.

The Dimetal Center. As intended in the design, the dimetal site lies at the bottom of a deep, water-filled pocket. In addition to the active site Mn(II) ions and protein side chains, a trilobate peak of electron density lies in a depression formed between the coordinating residues, E10 and 10′ (Figure 3A). This density is clearly observed in all three dimers of the asymmetric unit and has been interpreted as a dimethyl sulfoxide molecule, derived from the crystallization buffer (which contained 10% dimethyl sulfoxide). An acetate ion, derived from the manganese(II) acetate salt (present at 30 mM concentration in the

(30) Kanyo, Z. F.; Scolnick, L. R.; Ash, D. E.; Christianson, D. W. *Nature* **1996**, *383*, 554−557.
(31) Barynin, V. V.; Hempsted, P. D.; Vagin, A. A.; Antonyuk, S. V.; Melik-Adamyan, W. R.; Lamzin, V. S.; Harrison, P. M.; Artymiuk, P. J. *J. Biol. Inorg. Chem.* **1997**, *67*, 196.
(32) Antonyuk, S. V.; Melik-Adamyan, V. R.; Popov, A. N.; Lamzin, V. S.; Hempstead, P. D.; Harrison, P. M.; Artymyuk, P. J.; Barynin, V. V. *Cryst. Rep.* **2000**, *45*, 105−116.
(33) Lah, M. S.; Dixon, M. M.; Pattridge, K. A.; Stallings, W. C.; Fee, J. A.; Ludwig, M. L. *Biochemistry* **1995**, *34*, 1646−1660.

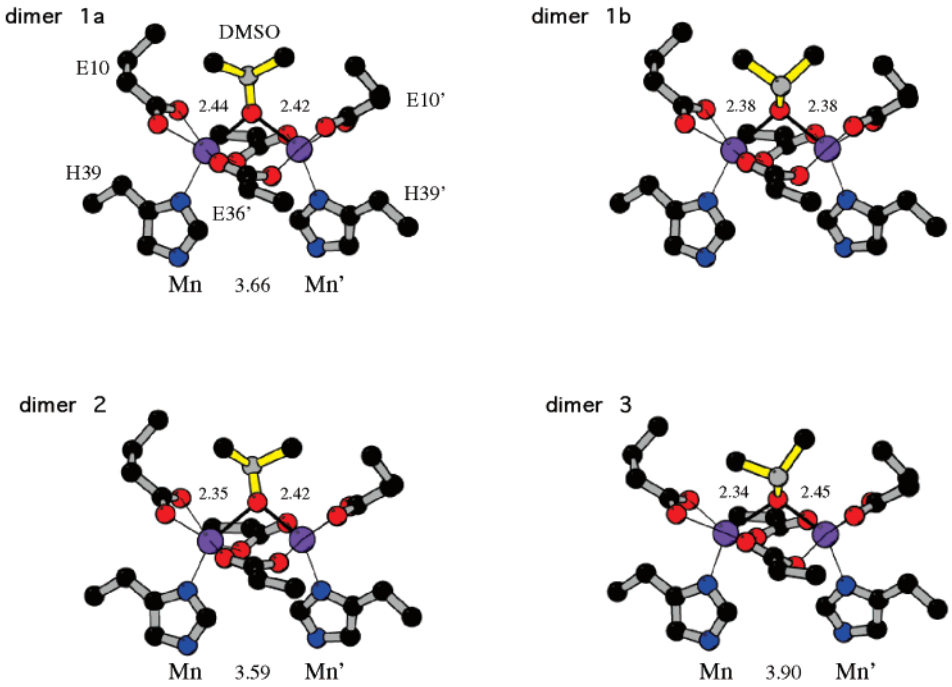

Figure 4. Metal−ligand coordination of the dimanganese centers of the independent L13A-DF1 dimers contained in the asymmetric unit of the unit cell. Also shown are the Mn^{2+}−Mn^{2+} distances along with the DMSO oxygen−Mn(II) distances. The active site structures were generated with Molscript.[69]

crystallization buffer), was considered as an alternative, because it was expected to be a better ligand than dimethyl sulfoxide. However, a pyramidal DMSO molecule fits better in the electron density (omit map) than a planar acetate ion (Figure 3A). Furthermore, the $F_o - F_c$ difference map calculated for the structure with acetate bound showed excess density at the central atom (data not shown). This indicated that a heavier atom (sulfur) could better fit the electron density map. The DMSO loosely coordinates the metal ions as a μ-1,1 bridge, with Mn−O distances of approximately 2.4 Å (Figure 4) in all three of the dimers. The electron density for the first dimer was consistent with two orientations for the ligand (Figure 4), each at 50% occupancy. The other two dimers appeared to bind their respective DMSO molecule in a single orientation, shown in Figure 4. In addition to DMSO, a number of ordered water molecules fill the pocket leading into the di-Mn(II) site. These water molecules fill the aqueous channel formed by the L13A and L13′A replacements in DF1 (Figure 5).

The presence of an exogenous bridging organic ligand in the di-Mn(II)-L13A-DF1 active site is well precedented in the active sites of structurally characterized diiron and dimanganese proteins. For example, dimethyl sulfoxide can coordinate directly to iron in the mixed valence state of methane monooxygenase.[34] An exogenous acetate molecule is observed in the diiron site of the hydroxylase component of methane monooxygenase (MMO)[15,35] which coordinates the metal ions in a η_2-bridging manner. It has been suggested that this ion may occupy the position normally occupied by substrates during a catalytic cycle.[15,35] Furthermore, crystallographic studies have also shown that formate, methoxide, and ethanol can occupy the same position (μ-ligand) at the diferric MMO metal center.[36,37] In addition, chloride ions, which reversibly inhibit dimanganese catalase from *Thermus thermophilus*, have been structurally observed to serve as μ-ligands.[32] Recently, an azide anion, which rescues the activity of the E238A mutant R2 protein of ribonucleotide reductase, has been structurally identified as a μ-ligand that replaces a mutated, bridging carboxylate ligand.[38]

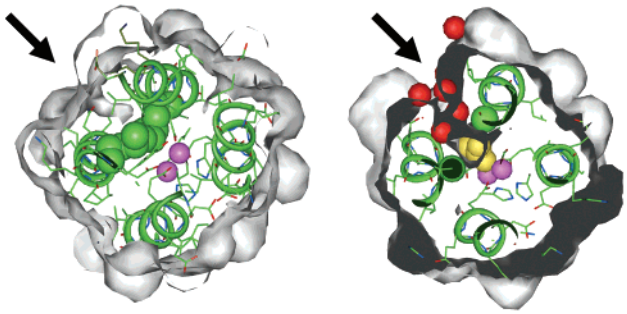

Figure 5. (Left) Top view of the active site cavity in DF1, highlighting the L13 and L13′ residues (green spheres), which block substrate access to the metal ions (violet spheres). (Right) Structure of the substrate access channel (indicated by black arrow) that results from the L13A and L13′A mutations. The yellow spheres highlight the dimethyl sulfoxide molecule, and the red spheres highlight the water molecules. These figures were generated with InsightII (BIOSYM, San Diego, CA).

The Mn−Mn distances in the three dimers range from 3.6 to 3.9 Å (Figure 4). These distances are within the range of intermetal ion distances observed in the di-Mn(II) forms of bacterioferritin (Mn−Mn distance = 4.0 Å)[16] and ribonucleotide reductase R2 (3.6−3.7 Å) (Figure 6), both of which have two μ-1,3 bridging carboxylate ligands.[14] Shorter distances are found in di-Mn(II) proteins with a single μ-1,3 carboxylate bridge and

(34) DeRose, V. J.; Liu, K. E.; Lippard, S. J.; Hoffman, B. M. *J. Am. Chem. Soc.* **1996**, *118*, 121−134.
(35) Rosenzweig, A. C.; Brandstetter, H.; Whittington, D. A.; Nordlund, P.; Lippard, S. J.; Frederick, C. A. *Proteins* **1997**, *29*, 141−52.
(36) Whittington, D. A.; Sazinsky, M. H.; Lippard, S. J. *J. Am. Chem. Soc.* **2001**, *123*, 1794−1795.
(37) Whittington, D.; Lippard, S. J. *J. Am. Chem. Soc.* **2001**, *123*, 872−838.
(38) Assarsson, M.; Anderson, M. E.; Hogbom, M.; Persson, B. O.; Sahlin, M.; Barra, A.-L.; Sjoberg, B.-M.; Nordlund, P.; Graslund, A. *J. Biol. Chem.* **2001**, *276*, 26852−26859.

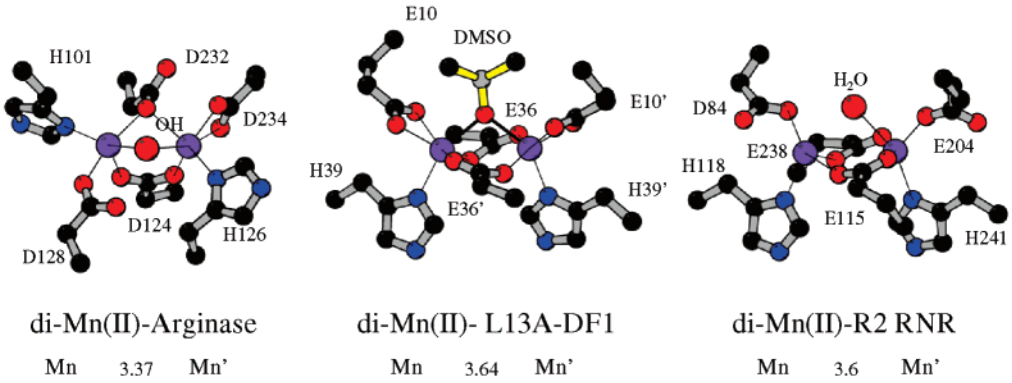

Figure 6. Metal centers of dimanganese-substituted proteins. The large red spheres correspond to a hydroxide molecule in the arginase structure (left) and a water molecule in R2 RNR (right). The Mn(II)−Mn(II) distances are shown below the structures. The figures were generated with Molscript.[69]

Table 3. Ligand−Metal Distances (Å) in the Active Sites of the Di-Mn(II)-L13A-DF1 Protomers in the Asymmetric Unit and Those in the Di-Zn(II)-DF1 Active Site

	dimer 1	dimer 2	dimer 3	di-Zn(II)-DF1	
E10, Mn1	2.30, 2.28	2.37, 2.23	2.19, 2.32	E10, Zn	2.0, 2.2
E10′, Mn′	2.32, 2.11	2.26, 2.33	2.29, 2.19	E10′, Zn′	2.1, 2.0
E36, Mn, Mn′	2.04, 2.11	2.08, 2.06	2.06, 2.07	E36, Zn, Zn′	2.1, 2.1
E36′, Mn, Mn′	2.12, 2.00	2.03, 2.09	2.05, 2.06	E36′, Zn, Zn′	2.1, 1.8
H39, Mn	2.31	2.19	2.23	H39, Zn	2.1
H39′, Mn′	2.24	2.24	2.26	H39′, Zn′	1.9
O(DMSO), Mn, Mn′	2.44, 2.42	2.35, 2.42	2.34, 2.45		
O(DMSO)′, Mn, Mn′	2.38, 2.38				

Table 4. Ligand−Metal Distances (Å) in the Metal Centers of Dimanganese-Substituted Proteins

di-Mn(II)-DF1-L13A		di-Mn(II)-arginase		di-Mn(II)-R2 RNR	
E10, Mn	2.30, 2.28	D128, Mn1	2.09	D84, Mn1	2.3
E10′, Mn′	2.32, 2.11	D234, Mn1	2.18, 2.41	E204, Mn2	2.0
E36, Mn, Mn′	2.04, 2.11	D232, Mn1, Mn2	2.38, 2.41	E238, Mn1, Mn2	2.1, 2.1
E36′, Mn, Mn′	2.12, 2.00	D124, Mn1, Mn2	2.15, 2.03	E115, Mn1, Mn2	2.2, 2.3
H39, Mn	2.31	H126, Mn2	2.12	H118, Mn1	2.2
H39′, Mn′	2.24	H101, Mn1	2.19	H241, Mn2	2.3
O(DMSO), Mn, Mn′	2.42, 2.40	OH, Mn1, Mn2	2.38, 2.41	H_2O, Mn1, Mn2	2.53, 2.79

two μ-1,1 bridging interactions such as di-Mn(II) catalase (3.3−3.6 Å, depending on the number and the nature of bridging anions)[32,39−41] and arginase.[30] Much shorter distances have been observed for di-Mn(III) forms of dimanganese catalase (2.7−3.1 Å) and small molecule active site mimics,[31,41] suggesting that the manganese is in the Mn(II) oxidation state in L13A-DF1. The Mn−Mn distances observed in L13A-DF1 are also consistent with those observed in di-Mn(II) model compounds with two 1,3 bridging carboxylate ligands.[41]

Diiron and dimanganese proteins show limited but functionally significant shifts in their coordination geometries in response to changes in the metal ions, their oxidation states, and the presence of exogenous ligands.[39,41−44] The most prominent difference between the di-Zn(II)-DF1 and di-Mn(II)-L13A-DF1 active site structures is the expansion of the coordination number from 5 to 6. Furthermore, as expected from the different atomic radii of Zn(II) and Mn(II) and from the increase in the coordination number, the distance between the protein ligands and the metal ions increases in the di-Mn(II) structure (Tables 3 and 4).[45,46] The metal ion−ligand distances increase by as much as 0.3 Å for H39 and the chelating E10 (and also H39′ and E10′) (Tables 3 and 4). The distances also increase for the bridging ligands E36 and E36′. These Mn(II)−ligand distances are very similar to those observed in the structures of the di-Mn(II) forms of RNR R2 and arginase (Table 4). There is also a rearrangement of the glutamate bridges in the di-Mn(II)-L13A-DF1 active site with respect to its di-Zn(II)-DF1 analogue. The planes of the two bridging carboxylates are rotated with respect to each other by an angle of approximately 12°, from a value of 32 ± 12° (Zn(II)) (mean and standard error over the dimers in the asymmetric unit) to a value of 44 ± 4° (Mn(II)).

There are some notable structural differences between the metal centers of di-Mn(II)-L13A-DF1 and those of the dimanganese-substituted R2 subunit of ribonucleotide reductase (di-Mn(II)-R2 RNR) and the dimanganese catalase from *T. thermophilus* (di-Mn(II)-Cat). One difference is the binding mode of the nonbridging carboxylate ligands. In both the R2 RNR and the catalase active sites, these carboxylates serve as

(39) Khangulov, S. V.; Pessiki, P. J.; Barynin, V. V.; Ash, D. E.; Dismukes, G. C. *Biochemistry* **1995**, *34*, 2015−2025.
(40) Meier, A. E.; Whittaker, M. M.; Whittaker, J. W. *Biochemistry* **1996**, *35*, 348−360.
(41) Law, N.; Caudle, M. T.; Pecoraro, V. L. *Adv. Inorg. Chem.* **1999**, *46*, 305−439.
(42) Rardin, R. L.; Tolman, W. B.; Lippard, S. J. *New J. Chem.* **1991**, *15*, 417−430.
(43) Tolman, W. B.; Liu, S.; Bentsen, J. G.; Lippard, S. J. *J. Am. Chem. Soc.* **1991**, *113*, 152−164.
(44) Dismukes, G. C. *Chem. Rev.* **1996**, *96*, 2909−2926.
(45) Lippard, S. J.; Berg, J. M. *Principles of Bioinorganic Chemistry*; University Science Books: Mill Valley, CA, 1994.
(46) da Silva, J. J. R. F.; William, R. J. P. *The biological chemistry of the elements*; Clarendon Press: Oxford, England, 1993.

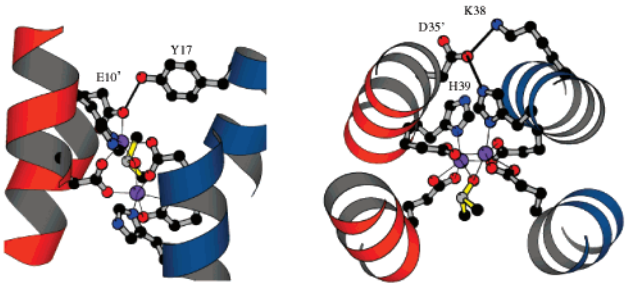

Figure 7. (Left) Second shell interactions involving Y17 and E10′. (Right) Hydrogen-bonded cluster involving K38, D35′, and the metal ligand, H39. The figures were generated with Molscript.[69]

monodentate ligands (Figure 6). In the L13A-DF1 active site both carboxylates are bidentate, chelating ligands. With respect to the bridging carboxylate ligands, DF1 is quite similar to di-Mn(II)-R2 RNR, which also has two 1,3 bridging carboxylates. By contrast, the di-Mn(II)-Cat structure has a single bridging carboxylate; the manganese ions are bridged by Glu70 and two solvent molecules.[32]

The structure of di-Mn(II)-L13A-DF1 also shows many similarities to di-Mn(II) arginase (although arginase is not a member of the four-helix bundle class of diiron and dimanganese proteins). As in di-Mn(II)-L13A-DF1, arginase has two bridging carboxylate ligands (Figure 6; D232 and D124). However, only D124 serves as a μ-1,3 bridge, and D232 is a μ-1,1 bridge. Arginase also has two nonbridging carboxylates, one of which is monodentate and the other bidentate. It will be interesting to determine how the differences between L13A-DF1 and these natural proteins translate into catalase activity. Arginase and RNR R2 support catalase activity, albeit at a much lower rate than does di-Mn(II)-Cat.[47−49]

Second Shell Interactions. Metal ion binding sites are often stabilized by groups that hydrogen bond to the primary ligands. These second shell ligands stabilize the structure of the metal binding site by precisely positioning the ligands in the primary coordination sphere and in the correct geometry.[50−54] It has also been shown that these second shell interactions can help to tune the electrochemical midpoint potential of redox-active metal ions.[55,56] As intended in the design, Y17 donates a second shell hydrogen bond to the nonbridging E10′ of the other monomer in each of the dimeric units (the same interaction exists between the symmetrically related pair, Y17′ and E10) (Figure 7). These interactions are observed for all six pairs (two quasi symmetry related pairs in each dimer) in the unit cell of the three dimers. The mean distance between the tyrosine phenolic oxygen and the glutamate carboxylate oxygen, (2.70 ± 0.05 Å (standard error), and the geometry are consistent with the formation of a hydrogen bond. Also consistent with the design, D35′ forms a hydrogen bond with the ligating H39 from a neighboring helix in the dimer (Figure 7). These interactions are also observed for all six pairs in the asymmetric unit, with a mean distance of 2.79 ± 0.03 Å, between the carboxylate oxygen of D35′ and the ϵ-N of H39. This distance is indicative of a reasonably strong hydrogen bond, possibly imparting partial imidazolate character to the histidine side chain.[51,55,57] Finally, the design of DF1 includes an intermonomer salt bridge between K38 of one unit and D35′ of a neighboring helix (Figure 7). This solvent-exposed interaction is observed in five of six monomers in the asymmetric unit. Interestingly, sequence analysis reveals that a similar primary ligand sphere−second shell hydrogen-bonded cluster is present in the active sites of methane monooxygenase,[35] ACP Δ^9-desaturase,[13] and other class II diiron-oxo proteins.[58,59] In these enzymes, the lysine residue (K38, L13A-DF1) is replaced by an arginine residue to form an Arg-Asp-His cluster.

There are some differences in several second shell interactions between di-Mn(II)-L13A-DF1 and di-Mn(II)-Cat.[60] Structurally analogous to the Tyr-Glu pair in di-Mn(II)-L13A-DF1 is a Lys-Glu interaction in di-Mn(II)-Cat. In addition, di-Mn(II)-Cat contains a His-Glu-His triad, in which Glu69 simultaneously interacts with both His ligands (H70 and H188), whereas two Asp-His pairs are present in the DF2 dimer.

Binding of Small Molecules to Di-Fe(III)-DF2. Although the crystallographic data described above provide evidence that the L13A and L13′A mutations result in small molecule (DMSO) and solvent access to the dimetal center, experimental solution data are also desirable. Because this helical bundle system has been designed to serve as a minimal model of both natural diiron and dimanganese proteins, it is of interest whether the conclusions concerning small molecule and solvent access to the metal center from the crystallographic studies with di-Mn(II)-L13A-DF1 would extend to the diiron derivative. To this end, we have examined the binding of azide, a spectroscopic homologue of the anionic dioxygen species,[1,2] and acetate,[60] a molecule known to inhibit manganese catalase, to the diferric form of DF2 (Figure 1C; a variant of L13A-DF1 with increased water solubility). Moreover, a large body of spectroscopic data exists for the diferric proteins, which allows comparison of our spectra with those of well-characterized small molecule compounds and proteins.[25,61]

The optical spectrum of di-Fe(III)-DF2 is shown in Figure 8. The spectrum of di-Fe(III)-DF2 is similar to those of proteins and inorganic complexes that contain Fe(III)−O−Fe(III) systems. As apparent with di-Fe(III)-DF2, these natural proteins and model complexes exhibit strong LMCT (oxo-Fe(III) ligand to metal charge transfer) absorption bands from 300 to 350 nm and much weaker bands between 400 and 700 nm (Figure 8).[20,21,59,62] The weaker bands between 400 and 700 nm may include contributions from charge-transfer bands and d−d ligand field transitions.[25,43,61] These di-Fe(III)-DF2 absorption bands are very similar to those observed in proteins in which the diferric-oxo unit has been structurally characterized, including ribonucleotide reductase R2 subunit,[18,19] stearoyl-acyl carrier

(47) Elgren, T. E. S.; T. L.; Marcoline, A. T.; Goldstein, J. I.; Bomann, A.; Penner-Hahn, J. *J. Inorg. Biochem.* **1996**, *67*, 337.
(48) Elgren, T. E.; Marcoline, A. T.; Goldstein, J. I. *J. Inorg. Biochem.* **1999**, *74*, 122−124.
(49) Shank, M.; Barynin, V.; Dismukes, G. C. *Biochemistry* **1994**, *33*, 15433−15436.
(50) Christianson, D. W.; Fierke, C. A. *Acc. Chem. Res.* **1996**, *29*, 331−339.
(51) Christianson, D. W.; Alexander, R. S. *J. Am. Chem. Soc.* **1989**, *111*, 6412−6419.
(52) Huang, C.-C.; Lesburg, C. A.; Kiefer, L. L.; Fierke, C.; Christianson, D. *Biochemistry* **1996**, *35*, 3439−3446.
(53) Kuo, J. M.; Chae, M. Y.; Raushel, F. *Biochemistry* **1997**, *36*, 1982−1988.
(54) Marino, S. F.; Regan, L. *Chem. Biol.* **1999**, *6*, 649−655.
(55) Gooden, D. B.; McRee, D. E. *Biochemistry* **1993**, *32*, 3313−3324.
(56) Vance, C. K.; Miller, A.-F. *J. Am. Chem. Soc.* **1998**, *120*, 461−467.
(57) Valentine, J. S.; Sheridan, R. P.; Allen, L. C.; Kahn, P. C. *Proc. Natl. Acad. Sci. U.S.A.* **1979**, *76*, 1009−1013.
(58) Fox, B.; Shanklin, J.; Somerville, C.; Munck, E. *Proc. Natl. Acad. Sci. U.S.A.* **1993**, *90*, 2486−2490. Ai, J.; Broadwater, J. A.; Loehr, T. M.; Sanders-Loehr, J.; Fox, B. G. *J. Bioinorg. Chem.* **1997**, *2*, 37−45.
(59) Fox, B. G.; Shanklin, J.; Ai, J.; Loehr, T. M.; Sanders-Loehr, J. *Biochemistry* **1994**, *33*, 12776−12786.
(60) Khangulov, S. V.; Goldfeld, M. G.; Gerasimenko, V. V.; Andreeva, N. E.; Barynin, V. V.; Grebenko, A. I. *J. Inorg. Biochem.* **1990**, *40*, 279−292.
(61) Kurtz, D. M. *Chem. Rev.* **1990**, *90*, 585−606.
(62) Dunn, J. B. R.; Addison, A. W.; Bruce, R. E.; Loehr, J. S.; Loehr, T. M. *Biochemistry* **1977**, *16*, 1743−1749.

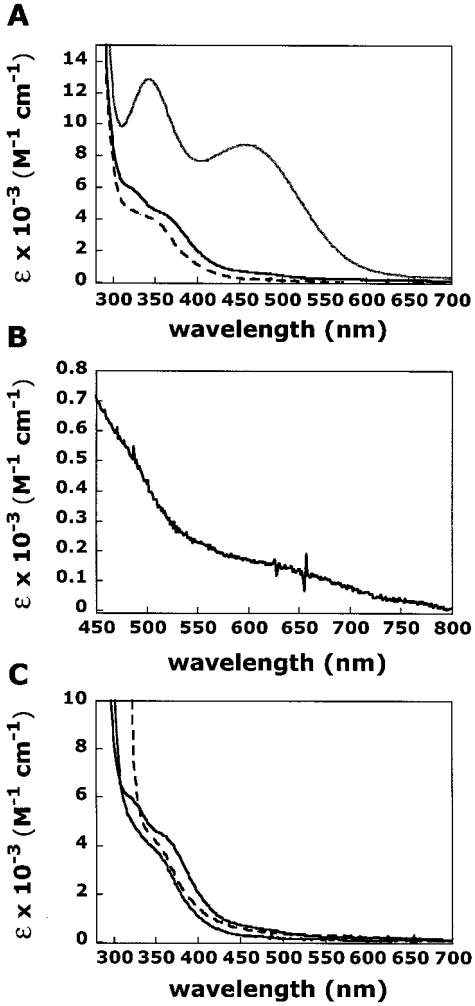

Figure 8. (A) Spectrum of di-Fe(III)-DF2 (solid black lines) and spectral changes that accompany the addition of the small molecules sodium azide (gray line) and sodium acetate (black dashed line). (B) Additional weaker di-Fe(III)-DF2 spectral features. (C) Spectral changes that accompany the addition of benzoic acid (gray line) and 4-hydroxybenzoate (black dashed line).

protein Δ^9-desaturase,[58] and methemerythrin.[21] The spectrum of the anaerobically Fe(II)-reconstituted DF2 shows no strong absorption bands above 280 nm (data not shown). However, the bands are present if the protein is aerobically reconstituted or if the anaerobic reconstituted complex is exposed to air.

The addition of sodium azide ion results in the appearance of two intense bands at 340 and 460 nm (Figure 8). The spectrum of the azide−di-Fe(III)-DF2 complex is nearly identical to the spectrum of the azide−di-Fe(III)-ACP Δ^9-desaturase complex, which contains strong absorption features at 345 and 450 nm (the extinction coefficient was not reported for the complex), and very similar to that of the azide−methemerythrin complex ($\epsilon_{326nm} \sim 6750$ M^{-1} cm^{-1}, $\epsilon_{446nm} \sim 3700$ M^{-1} cm^{-1}).[20,21,58,59,62] The removal of the ligand by gel filtration restores the original absorption bands, indicating that the diiron-oxo site is still intact. A titration of di-Fe(III)-DF2 with azide (Figure 9) results in a binding curve with a Hill coefficient of 1.5, suggesting that more than one azide ion binds to thermodynamically interacting sites. Similarly, two binding sites have been spectroscopically observed for RNR R2.[63] The binding of more than one azide anion to di-Fe(III)-DF2 is also suggested

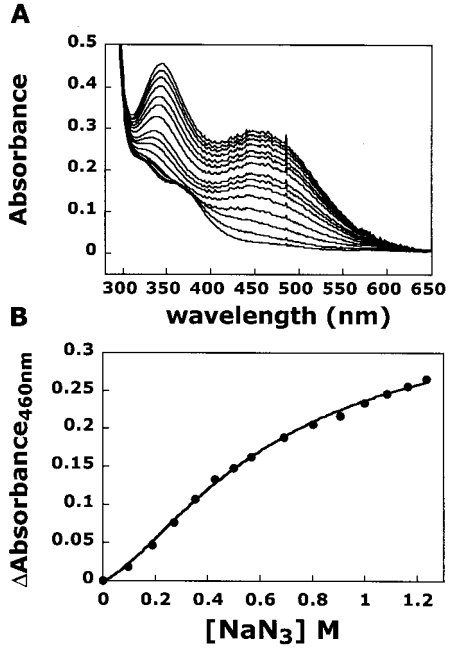

Figure 9. Titration with sodium azide. (A) UV−vis absorption spectra that accompany successive additions of sodium azide to di-Fe(III)-DF2. (B) Increase in absorbance at 460 nm as a function of ligand concentration. The data were fit to the Hill equation: $[NaN_3]^N/(K + [NaN_3]^N)$. The parameters obtained from the fit were as follows: $N = 1.5 \pm 0.1$, $K = 0.56$ M, and $R = 0.99$.

by the high extinction coefficient for the complex ($\epsilon_{340nm} \sim 12\,800$ M^{-1} cm^{-1}, $\epsilon_{446nm} \sim 8700$ M^{-1} cm^{-1}). This value is about twice that of the azide−methemerythrin complex which is known to bind one anion (see above).[20,21,62] The crystal structures of the azide-bound diiron-oxo proteins, methemerythrin[64,65] and the R2 subunit of ribonucleotide reductase (F208A/Y122F),[66] indicate that the azide anion binds to one of the iron ions in the metal center in a nonbridging mode. The similarities in the spectral properties of the azide-bound di-Fe(III)-DF2 and azidomethemerythrin suggest that the ion may bind in a similar manner.

The addition of sodium acetate results in significantly different spectral changes than when azide is added (Figure 8). The intensity of the absorption bands at 330, 360, and 475 nm of the di-Fe(III)-DF2 spectrum decreases upon sodium acetate addition (to a final concentration of ~1.5 M). In addition, the bands at 330 and 360 nm become less well resolved. These spectral changes suggest that acetate binds to the protein and alters the ligand field of the dimetal center. Although these optical spectral changes are small, acetate binding to the metal center is also supported by changes in the circular dichroism spectrum (data not shown). The addition of the more hydrophobic benzoate or 4-hydroxybenzoate anions (final concentration of approximately 0.5 M) results in spectral changes similar to those occurring upon the formation of the acetate−di-Fe(III)-DF2 complex, suggesting that the carboxylate groups of these ligands interact with the metal center. As with azide, the removal of the carboxylate-containing ligands by gel filtration restores the original spectrum.

(63) Pulver, S. C.; Tong, W. H.; Bollinger, J. M.; Stubbe, J.; Solomon, E. I. *J. Am. Chem. Soc.* **1995**, *117*, 12664−12678.

(64) Stenkamp, R. E.; Siekker, L. C.; Jensen, L. H. *J. Mol. Biol.* **1978**, *126*, 457−466.

(65) Holmes, M. A.; Stenkamp, R. E. *J. Mol. Biol.* **1991**, *220*, 723−737.

(66) Andersson, M. E.; Högbom, M.; Rinaldo-Matthis, A.; Andersson, K. K.; Sjöberg, B.-M.; Nordlund, P. *J. Am. Chem. Soc.* **1999**, *121*, 2346−2352.

Because the ligand spheres of each active site ferric ion of di-Fe(III)-oxo-DF2 are presumably saturated (six ligands—five protein-based ligands and an oxo bridge) without the exogenous ligands, it appears that one (or more) of the protein-based ligands in the metal center may be able to change its coordination mode in order to accommodate the addition of the azide ion. Changes in coordination mode of active site ligands in natural diiron proteins are well precedented, as they have been structurally characterized in methane monooxygenase[15,37] and in the R2 subunit of ribonucleotide reductase.[66,67] In all cases, the ligating modes of the active site carboxylate ligands have been shown to be flexible. In fact, three of the four liganding carboxylates in the ribonucleotide reductase system have been shown to exhibit this type of activity (also termed carboxylate shifts),[42] whereas one of the four is mobile in methane monooxygenase. This flexibility is not surprising as carboxylate ligands are able to adopt monodentate and bidentate modes (syn or anti) of coordination. In addition, the glutamate side chain has high conformational flexibility due to additional methylene groups, which could lower the energetic barrier to changing coordination modes. Carboxylate-coordinating changes have been postulated to serve as an important catalytic redox mechanism as it allows for facile changes in the metal coordination spheres. Furthermore, different coordination modes may be important for stabilizing different metal ion oxidation states. Indeed, the active site metal ions cycle between +2, +3, and/or +4 oxidation states during the catalytic hydroxylation of hydrocarbons by methane monooxygenase and during the generation of the tyrosyl radical in the R2 subunit of ribonucleotide reductase.[9,68] The binding of exogenous ligands to the active site of the R2 subunit of ribonucleotide reductase has also been shown to result in a carboxylate shift.

Conclusion

The primary goal of this work was to elaborate the stable, but nonfunctional DF1 into a protein with a substrate access channel leading to the carboxylate-bridged dinuclear metal center. The risk of this endeavor would be to decrease the driving force for folding due to the removal of buried hydrophobic residues. Fortunately, the idealized design of DF1 imparted sufficient stability to tolerate significant changes, both in amino acid sequence as well as metal ion, without affecting its overall fold. The three-dimensional structures of the metal binding sites of the di-Zn(II)-DF1 and di-Mn(II)-L13A-DF1 are very similar, indicating that the introduction of the access channel and changing the metal ion from Zn(II) to Mn(II) did not greatly affect the structure of the protein. These data are consistent with previous studies, indicating that the binding of metal ions enhances the stability of DF2 but is not essential for the integrity of the protein fold.[17] Further, the NMR solution structure of apo-DF1 is nearly identical to the crystal structure of the di-Zn(II) complex (unpublished results).

Our spectroscopic studies of DF2 suggest that the water-filled, active site pocket, observed in the crystal structure of di-Mn(II)-L13A-DF1, is also present in di-Fe(III)-DF2 in aqueous solution. These experiments indicate that the dinuclear metal binding site of the diferric form of the protein is accessible to azide- and carboxylate-containing molecules. These ligands bind to the diferric center at concentrations similar to those observed for other diiron and dimanganese proteins and induce similar spectroscopic changes. Thus, the DF1 family of proteins appears to adopt a robust tertiary structure that is resistant to changes in both amino acid sequence and the bound metal ion.

These studies have now established the feasibility of building an active site cavity into the structure of a highly simplified diiron, dimanganese protein. Thus, future studies with DF1 will be aimed at determining how changes in the polarity, solvent accessibility, and electrostatic potential surrounding the dimetal center will affect its electrochemical midpoint potential and chemical reactivity, with the ultimate goal being the elaboration of catalysts capable of mediating a variety of oxygen-dependent reactions.

Acknowledgment. L.D.C. and H.W. contributed equally to this work. We thank Flavia Nastri for critically reading the manuscript. We also thank the Italian Ministry of University and Scientific Research (PRIN MM03185591) and the National Institutes of Health (GM54616) for financial support. This work was also supported by postdoctoral fellowships from the NSF (to H.W.) and from CIRCMSB (to L.D.C.). Finally, we thank Omar Zgheib for technical assistance.

Supporting Information Available: Coordinates have been deposited in the RCSB Data Bank, access numbers 1JM0 for the form **1** and 1JMB for the form **2**.

JA010506X

(67) Logan, D. T.; deMare, F.; Persson, B. O.; Slaby, A.; Sjoberg, B. M.; Nordlund, P. *Biochemistry* **1998**, *37*, 10798−10807.
(68) Waller, B. J.; Lipscomb, J. D. *Chem. Rev.* **1996**, *96*, 2625−2657.
(69) Kraulis, P. J. *J. Appl. Crystallogr.* **1991**, *24*, 946−950.